NANO LETTERS
Cite This: Nano Lett. 2018, 18, 6094−6099
Letter
pubs.acs.org/NanoLett

Atomic-Scale Probing of Reversible Li Migration in 1T-$V_{1+x}Se_2$ and the Interactions between Interstitial V and Li

Ruiwen Shao,[†] Shulin Chen,[†,‡] Zhipeng Dou,[†,§] Jingmin Zhang,[†] Xiumei Ma,[†] Rui Zhu,[†] Jun Xu,[†] Peng Gao,*[,†,∥,⊥] and Dapeng Yu[†,⊥,#]

[†]Electron Microscopy Laboratory, School of Physics, Peking University, Beijing 100871, China
[‡]State Key Laboratory of Advanced Welding and Joining, Harbin Institute of Technology, Harbin 150001, China
[§]Key Laboratory for Micro-/Nano-Optoelectronic Devices of Ministry of Education, School of Physics and Electronics, Hunan University, Changsha 410082, China
[∥]International Center for Quantum Materials, School of Physics, Peking University, Beijing 100871, China
[⊥]Collaborative Innovation Center of Quantum Matter, Beijing 100871, China
[#]Department of Physics, South University of Science and Technology of China, Shenzhen 518055, China

Supporting Information

ABSTRACT: Ionic doping and migration in solids underpins a wide range of applications including lithium ion batteries, fuel cells, resistive memories, and catalysis. Here, by in situ transmission electron microscopy technique we directly track the structural evolution during Li ions insertion and extraction in transition metal dichalcogenide 1T-$V_{1+x}Se_2$ nanostructures which feature spontaneous localized superstructures due to the periodical interstitial V atoms within the van der Waals interlayers. We find that lithium ion migration destroys the cationic orderings and leads to a phase transition from superstructure to nonsuperstructure. This phase transition is reversible, that is, the superstructure returns back after extraction of lithium ion from $Li_yV_{1+x}Se_2$. These findings provide valuable insights into understanding and controlling the structure and properties of 2D materials by general ionic and electric doping.

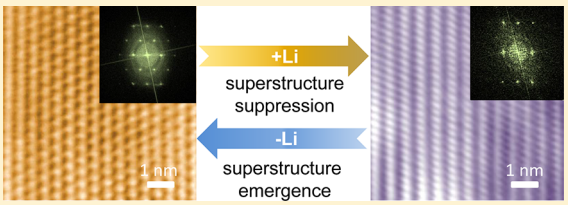

KEYWORDS: *Transition metal dichalcogenide, ion migration, order−disorder transition, in situ TEM, structure ordering*

Layered transition metal dichalcogenides (TMDs) have attracted great research interest in areas of energy conversion and storage devices,[1] nanoelectronics,[2] optoelectronics,[3] and electrocatalysis[4] due to their unique physical and chemical properties.[5,6] These two-dimensional (2D) TMD MX_2 (M = Mo, W, Ti, etc.; X = S, Se, Te) materials are composed of hexagonally coordinated X−M−X atomic slabs.[7] Atoms within each slab are strongly bonded by covalent interaction while adjacent layers are predominantly bonded by weaker van der Waals force. The large space between the slabs permits intercalation of guest atoms and even molecules therein to form intercalation compounds (new phases).[8,9] Therefore, these layer-structured TMDs can serve as an ideal platform for probing the intricate interplay wherein the structure and properties are susceptible to guest species intercalation.[10−17]

Indeed, the controllable ion intercalation provides powerful means to tune the properties.[18−24] In the past few decades, tremendous efforts have been devoted to studying these layered materials by intercalating organic molecules and alkali metals.[8−27] With foreign species intercalated within the interlayers of the host chalcogenide, the bonding interactions between layers are no longer van der Waals. As a result, the newly formed intercalated phases usually have very different physical and chemical properties compared with the pristine ones. For example, previous experiments demonstrated a phase transition from pristine semiconducting 2H-MoS_2 to the metallic 1T-MoS_2 upon alkali ions intercalation.[10,15] Generally, the ionic liquid gating was widely used to control the ionic doping in TMDs, enabling various interesting properties, including superconductivity,[28,29] ambipolar transport,[30,31] electric field control of spin polarization,[32] and circularly polarized electroluminescence.[33] Because the atomic structure and chemistry of these layered structures dictate the properties, it is important to probe the structural evolution during ion intercalation and the interactions between intercalants. The recent advancements of in situ transmission electron microscopy (TEM) allow us to track the ion migration-induced solid-state phase transformation at an atomic scale and millisecond,[34−37] providing unprecedented opportunities to explore the intercalation chemistry.[10−16]

Here, we use an in situ high-resolution TEM (HRTEM) technique to real-time track the foreign Li insertion and extraction processes in 1T-$V_{1+x}Se_2$ (vanadium diselenide) nanostructures and monitor the structural evolutions. The nonstoichiometric VSe_2, that is, $V_{1+x}Se_2$, tends to form self-

Received: August 1, 2018
Published: August 24, 2018

DOI: 10.1021/acs.nanolett.8b03154
Nano Lett. 2018, 18, 6094−6099

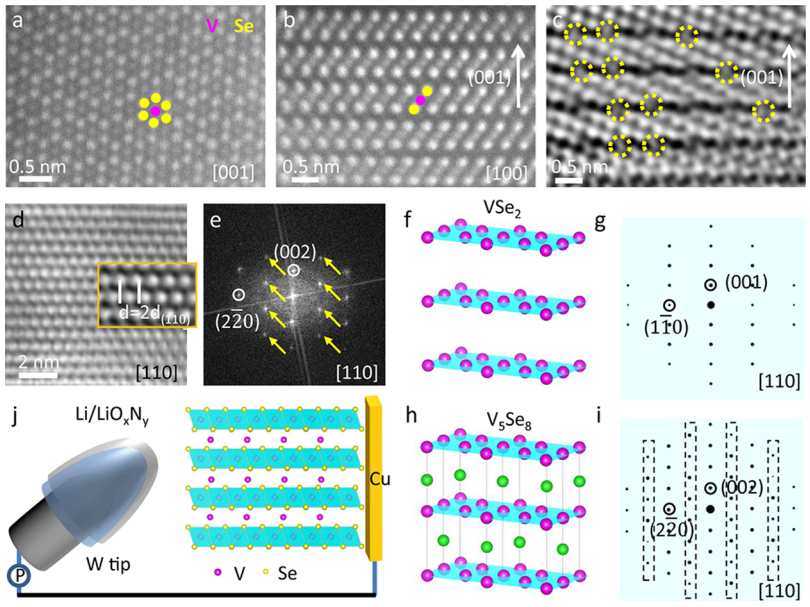

Figure 1. TEM characterization and schematic of in situ TEM setup. (a,b) Atomically resolved HAADF image of 1T-VSe_2 (x = 0) viewed from the (a) [001] and (b) [100] directions. (c) The inverse FFT image of the atomically resolved HAADF image of $V_{1+x}Se_2$ viewing perpendicular to [001] direction. The interstitial V atoms are marked by yellow circles. (d) The HRTEM image of the domain with the nonstoichiometric phase V_5Se_8 (x = 0.25) viewed from the [110] direction and (e) the corresponding FFT pattern. The distance of the $(1\bar{1}0)$ plane of V_5Se_8 (x = 0.25) measured from the HRTEM is ~0.58 nm, which is twice the distance of the $(1\bar{1}0)$ plane (2.9055 Å) of the 1T-VSe_2 (x = 0). The superstructure spots induced by interstitial V atoms are marked by yellow arrows. (f) The atomic model for the VSe_2 (x = 0) phases and (g) the corresponding simulated ED pattern along the [110] direction. Sulfur atoms in the 3D view image were omitted for clear identification of intercalation sites. (h) The atomic model for the V_5Se_8 (x = 0.25) phase and (i) the corresponding simulated ED pattern along the [110] direction. Note that the superstructure spots (marked by black dashed rectangle) can be observed in V_5Se_8 (x = 0.25) due to the ordered intercalated V atoms (green balls) between the VSe_2 layers (magenta balls), as shown in (h). (j) The schematic shows the in situ TEM measurement setup consisting of a 1T-$V_{1+x}Se_2$ nanosheet, a metallic lithium probe, and a thin passivation layer of LiO_xN_y acting as the solid-state electrolyte.

intercalated compounds, such as V_3Se_4 and V_5Se_8.[38−45] For TMDs, when going to the right of the periodic table the d levels (a d-subshell contains d-orbitals inside an atom's electron shell) progressively decrease in energy and may enter the sulfur or selenium p valence band.[46] Then the d level will be filled at the expense of the valence band, which means that the cations M^{4+} are reduced and the anions X^{2-} are oxidized, resulting in the instability of the compound.[46] In the cation rich compositions, the ordering of the interstitial cations provides further stability for the nonstoichiometric phases.[47] In general, these intermediate compounds can be regarded as a superstructure consisting of ordered interstitial V atoms within the van der Waals gaps in a MX_2-type structure.[48−50] Such self-intercalation effect provides an additional degree of freedom in creating a series of nonstoichiometric materials beyond the existing ones, as well as in tuning the electronic/magnetic properties of hosts.[38,40,51,52] For example, the magnetic susceptibility of $V_{1+x}Se_2$ shows a Curie−Weiss like behavior at low temperatures which originates from an excess of V ions orderly locating in the van der Waal gaps[53−56] because each interstitial V ion produces a net paramagnetic moment of 2.5 Bohr magnetons.[55,56] It has been reported that annealing is an effective method to control the ordering of the cations in the structure.[57,58] By increasing the temperature, the low-temperature ordered phase of these interstitial cation ions gradually loses the degree of order to the high-temperature disordered phase, accompanied by dramatic changes occurring in the magnetic and electronic properties.[59−61] However, controlling the interstitial V ordering through ionic doping and thus further tuning the magnetic/electronic properties has been rarely explored and motivated our present study.

We observe the pristine 1T-$V_{1+x}Se_2$ nanosheets possess a spontaneous superstructure due to the periodical interstitial V atoms locating within the van der Waals interlayers. During the lithium ion migration within this nanostructure, the strong charge interactions between interstitial V and foreign Li destroys the V orderings to form nonsuperstructured $Li_yV_{1+x}Se_2$. The superstructure returns back after lithium ion extraction from $Li_yV_{1+x}Se_2$, indicating that this phase transition is reversible. These observations suggest that the cation ordering in $V_{1+x}Se_2$ can be effectively controlled by the foreign ionic doping. Because the ionic doping is a common technique to tune the properties of 2D materials, the present findings of intricate interplay between interstitial cation and foreign intercalants driven structural transition provide valuable insights into understanding the underlying mechanisms of ionic doping-controlled phase transformations and properties and shed lights on the design of new materials and devices through such technique.

The 1T-$V_{1+x}Se_2$ thin-sheet samples used in this study were cleaved from a bulk crystal by mechanical exfoliation. Small domains with superstructures (e.g., V_5Se_8 (x = 0.25) and V_3Se_4 (x = 0.5)) randomly distribute in the 1T-VSe_2 (x = 0) matrix (see Figure S1), which is consistent with the literatures.[38−45] Figure 1a,b is atomically resolved high-angle annular dark-field scanning transmission electron microscopy (HAADF-STEM) images of VSe_2 (x = 0) nanostructure along the direction of [001] and [100], respectively. No interstitial V atoms have been observed in the VSe_2 (x = 0) region. However, in the cation rich regions, viewing perpendicular to the same direction, the interstitial V atoms can be seen, as shown in Figure 1c. These interstitial cations forming superstructure can

DOI: 10.1021/acs.nanolett.8b03154
Nano Lett. 2018, 18, 6094−6099

produce extra spots in the diffraction pattern or stripes in the HRTEM image (in Figure 1d,e). The electron diffraction (ED) simulations confirm one of the superstructures is V_5Se_8 (x = 0.25, JCPDS Card No. 18-1455), and another nonstoichiometric phase V_3Se_4 (x = 0.5, JCPDS Card No. 17-0217) has also been observed in Figure S2. The corresponding atomistic models of 1T-VSe_2 (x = 0) and V_5Se_8 (x = 0.25) are shown in Figure 1f,h. The detailed structure parameters are shown in Table S1. The energy disperse spectroscopy (EDS) analysis indicates the atomic ratio of V to Se is ~(1.27 ± 0.02):2, further confirming the superstructure is V_5Se_8 (x = 0.25), as shown in Figure S3. In situ TEM method is used to insert and extract Li ions from 1T-$V_{1+x}Se_2$ and real-time track the structural evolution during lithium migration. Figure 1j shows the in situ TEM setup consisting of 1T-$V_{1+x}Se_2$, and Li metal coated with a passivation layer LiO_xN_y, acting as a solid-state electrolyte (see Experimental Section for details).

Then HRTEM image series were recorded to reveal the local structural evolutions during lithium intercalation and extraction in 1T-$V_{1+x}Se_2$. Figure 2 shows the lithium ion insertion

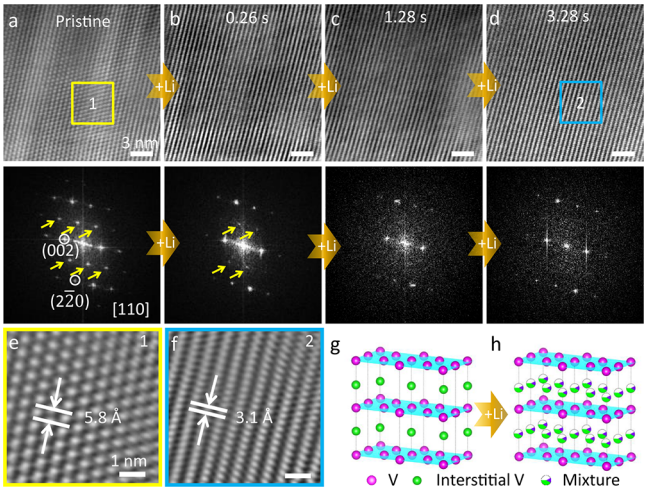

Figure 2. Tracking lithium insertion process in V_5Se_8 (x = 0.25) nanosheet in real-time. (a) HRTEM image of V_5Se_8 (x = 0.25) seen along the [110] direction and corresponding FFT pattern below. (b–d) The structural evolution during Li insertion and the corresponding FFT patterns. (e,f) Enlarged inverse FFT images corresponding to the squares in (a,d). (g,h) A schematic model of the structural transformation of the V_5Se_8 (x = 0.25) -type phase to the $Li_yV_5Se_8$ (x = 0.25) -type phase. Selenium atoms in the 3D view image were omitted for clear identification. Magenta balls represent the intralayer V atoms. Green balls represent self-intercalated V atoms. Three-color balls represent the mixture of V, Li atoms, and vacancies, and they distribute randomly in the van der Waals gaps.

processes within a V_5Se_8 (x = 0.25) domain. Such layered V_5Se_8 (x = 0.25) can be viewed as a VSe_2 structure intercalated with ordered V atoms, which has a monoclinic structure, space group $P2/m$. The HRTEM image and the corresponding fast Fourier transform (FFT) pattern seen along the [110] direction in Figure 2a shows additional superstructure spots marked by yellow arrows in the pristine structure compared to the ideal ED pattern of 1T-VSe_2 (x = 0) in Figure 1f, indicating a local structural ordering of the interstitial V atoms. Lithium insertion occurs spontaneously as soon as the solid-state electrolyte probe contacts with V_5Se_8 nanosheet. Upon Li intercalation, the extra superstructure spots like {1$\bar{1}$1} become weaker in Figure 2a–d and finally disappear completely. An enlarged inverse FFT image in Figure 2f that corresponds to the light blue region in Figure 2d shows the distance of stripes becomes ~0.31 nm, which is slightly larger than half of that in the pristine state in Figure 2e due to the lattice expansion induced by lithium intercalation. This structure after lithium intercalation is found to be similar to 1T-VSe_2 (x = 0, space group $P\bar{3}m1$), indicating that the ordering of the interstitial V atoms has been destroyed. The lithium insertion is further confirmed by electron energy loss spectroscopy (EELS) measurement, as shown in Figure S4. Figure 2g,h shows the order–disorder transition during lithium intercalation. Lithium insertion destroys the ordering of interstitial V atoms in the van der Waals gap (green balls), leading to the disappearance of the superstructure spots. In accordance with the present results, lithium insertion induced order–disorder transition process within a V_3Se_4 (x = 0.5) domain is shown in Figure S5. Besides, more lithium ions inserting into $V_{1+x}Se_2$ (by using a larger external voltage) leads to a conversion reaction, forming metal V and Li_2Se as shown in Figure S6.

Once the lithiation in 1T-$V_{1+x}Se_2$ is controlled within the range of intercalation, the lithium ions in $Li_yV_{1+x}Se_2$ can be extracted and the superstructure can be recovered as shown in Figure 3. In contrast to the fast lithium insertion process

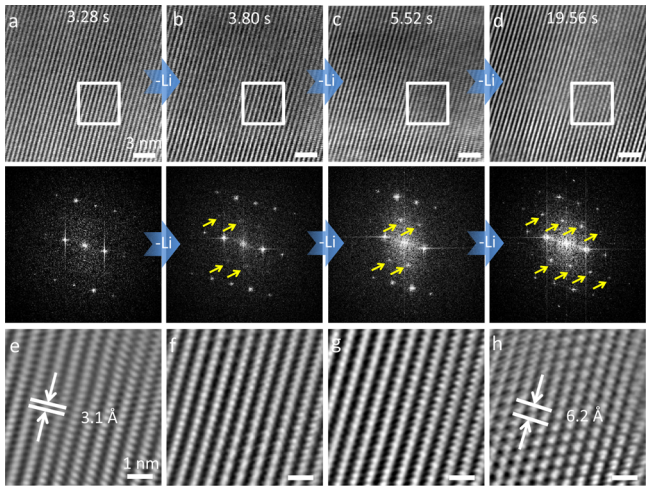

Figure 3. Tracking the lithium extraction process in V_5Se_8 (x = 0.25) nanosheet. (a) HRTEM image of the $Li_yV_5Se_8$ (x = 0.25) nanosheet after lithium insertion and corresponding FFT pattern below. (b–d) The structural evolution during Li extraction and the corresponding FFT patterns. (e–h) Enlarged inverse FFT images corresponding to the white squares in (a–d).

(Figure 2a–c), Li extraction (Figure 3a–d) is much slower. During the extraction under 1 V voltage, the superstructure spots in the FFT pattern reappear and fully recover subsequently, indicating the order–disorder transition is reversible. Note that the interplanar distance of the recovered phase ~0.62 nm in Figure 3h does not return to its original state (~0.58 nm), probably due to some Li still remaining in the structure. Figure 3e–h shows the enlarged inverse FFT images corresponding to the white squares in Figures 3a–d. Bright-dark strips along the (2$\bar{2}$0) direction are observed before the full recovery of the superstructure, consistent with the reappearance of the superstructure spots in FFT patterns. Usually after the extraction of Li, the superstructure returns as shown in Figure 2 and Figure S7. However, formation of new

DOI: 10.1021/acs.nanolett.8b03154
Nano Lett. 2018, 18, 6094–6099

superstructures after the lithium ion extraction from the $Li_yV_{1+x}Se_2$ that is different from the pristine one is also observed in Figure S8.

Consecutive selected area electron diffraction (SAED) patterns were also recorded to monitor the overall structural evolution upon Li intercalation (Figure 4a–h). The SAED

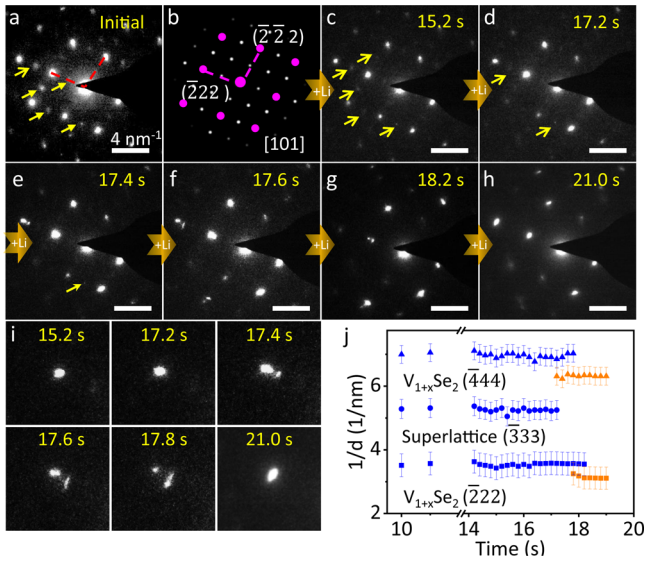

Figure 4. Consecutive SAED patterns during Li intercalation. (a) SAED pattern of a pristine V_5Se_8 (x = 0.25) nanosheet with viewing direction of [101] shows extra superstructure spots, marked by yellow arrows. (b) The simulated ED pattern of the single crystal V_5Se_8 (x = 0.25) viewing along the [101] direction. (c–h) The evolution of SAED patterns during Li intercalation. (i) The split process of the diffraction spot (4̄44). (j) The lithium insertion induced lattice expansion is measured from the diffraction spot of (2̄22) and (4̄44)-V_5Se_8 and superstructure spot (3̄33). Blue: pristine phase. Orange: lithium intercalated phase. Square: spot (2̄22). Triangle: spot (4̄44). Circular: superstructure spot (s33).

pattern in Figure 4a is recorded from a pristine V_5Se_8 (x = 0.25) nanosheet viewing along the [101] direction. The SAED pattern in Figure 4a shows additional superstructure spots induced by interstitial V atoms, compared to the simulated ED pattern (Figure 4b), in which the hexagonal Bragg peaks of VSe_2 layers are marked by magenta circles. Upon lithium intercalation, the superstructure diffraction spots become weaker and disappear completely at 17.4 s (Figure 4c–h). Figure 4i shows the split process of the diffraction spot (4̄44). Figure 4j shows the disappearance process of the superstructure spot (3̄33) and the split of the diffraction spots (2̄22) and (4̄44). The split of (2̄22) refection between pristine and intercalated phase is measured to be ~11.8 ± 4.3% in Figure 4g, which originates from the lithium intercalation induced lattice expansion.

For vanadium diselenide and vanadium sulfide, the tendency to form self-intercalated compounds $M_{1+x}X_2$ is well-known[38−45,62−64] because for these cation-rich compounds the interstitial atoms in the van der Waals gap of the layers improve structural stability.[65] So far the structural studies on the system have been performed and the structures of representative compounds such as V_5Se_8, V_3Se_4, and V_7Se_8 were reported.[32,66] The interstitial V atoms have an important influence on the electric transport,[30,31] magnetic properties,[32] and circularly polarized electroluminescence.[33]

The order−disorder transition can be understood in terms of electrochemical potential, including temperature[57,58] and pressure[67,68] and the effect of Coulomb interactions between the interstitial V ions and foreign Li ions. It has been reported that various phase transitions of these self-intercalated compounds $M_{1+x}X_2$ can be induced by annealing[57,58] or pressure.[67,68] Previous X-ray measurements revealed that in $V_{1+x}S_2$ and $V_{1+x}Se_2$ the order arrangement of the interstitial cation atoms at low temperatures becomes disordered at higher temperatures.[57,58] The V_5Se_8-type transforms into the V_3Se_4-type structure and finally into the nonstoichiometric VSe_2-type (CrI_2 structure) on heating.[57] Similarly, Nakazawa et al.[69] reported that above 800 °C, V_5S_8 transforms to a high temperature phase with a CdI_2-type structure. Within the CdI_2 structure, the octahedral sites in the vacancy layer become equivalent, that is, vacancies and cations should distribute randomly within this layer, resulting in the loss of the 2D supercell. Moreover, another self-intercalated TMD system, $Cr_{3\pm x}Se_4$, shows a reversible transition from the monoclinic Cr_3Se_4-type to the CrI_2-type structure during annealing.[58] These transitions between the disordering and ordering of interstitial V atoms have been qualitatively explained by a statistical thermodynamic treatment.[48]

On the other hand, in intercalation compounds, such as graphite, TMDs, and lithium battery materials, the guest atoms, notably Li, can exhibit a variety of ordered structures and order−disorder transitions under chemical/electrochemical conditions. Ordering of lithium and order−disorder transitions have been first proposed in intercalation compounds of layered chalcogenides such as Li_xTiS_2[70] and Li_xTaS_2.[71] Lithium ions are constrained to occupy certain sites preferentially as a result of long-range, repulsive, Coulomb interactions among lithium ions, which leads to the formation of superlattices at various lithium contents parallel to the transition metal layers.[70,71] Further lithium intercalation destroys the ordering and thus the vacancies and cations distribute randomly. First direct experimental evidence of lithium ordering is the presence of superstructures in the ED patterns of layered Li_xNiO_2.[72] Subsequently ED and TEM imaging have successfully revealed order−disorder phenomena of lithium and vacancy in layered Li_xCoO_2 electrode materials.[73]

Therefore, now we can understand the mechanism of cation ordering and disordering transition in 1T-$V_{1+x}Se_2$ in this study. First, the V ions can be mobile under external excitations, such as high temperature, and pressure. Second, the inserted lithium ions can have strong Coulomb interactions with the V ions. Third, the electrochemical potential drives the lithium migration in the 1T-$V_{1+x}Se_2$, during which the interactions between Li and V ions further drive the V migration, destroying the ordering of V atoms. After removing most of the lithium ions and thus leaving most of octahedral sites unoccupied, the structure tends to return back to the original state with V ordering, consistent with the annealing/cooling experiments,[57,58] which can be expected by thermodynamic analysis.[48]

In summary, we track the phase transition during lithium ion insertion and extraction in the van der Waals interactions dominated 1T-$V_{1+x}Se_2$ nanostructures in real-time and with lattice fringe resolution. The 1T-$V_{1+x}Se_2$ adopts lithium ions between the sulfide layers, which destroys the local ordering of interstitial V atoms. The lithium ions in $Li_yV_{1+x}Se_2$ can be extracted and the superstructure returns after lithium ion

DOI: 10.1021/acs.nanolett.8b03154
Nano Lett. 2018, 18, 6094−6099

extraction from $Li_yV_{1+x}Se_2$, once the lithiation is controlled within the range of intercalation. The order−disorder transition of V atoms further influences the magnetic and electronic properties. These observations can help us to understand the Li and V diffusion mechanism and the interplay between lattice and charge (chemical dopants) in TMDs. Besides the heating and pressure, the ionic doping provides a new pathway to control the structure and properties of TMDs.

Experimental Section. *In Situ TEM Experiments.* The 1T-$V_{1+x}Se_2$ nanosheets with layered structure were mechanically peeled off from a single crystal by using a half TEM Cu grid to scratch the surface of 1T-$V_{1+x}Se_2$ crystal. The Cu grid acts as one current collector and 1T-$V_{1+x}Se_2$ is considered to be working electrode. The typical thickness of 1T-$V_{1+x}Se_2$ nanosheet varies from a few nanometers to tens of nanometers. Lithium metal (acting as the counter electrode) was coated onto a sharp grounded tungsten probe. Typically, the diameters of W tips are smaller than 200 nm (Figure S9). All of the components were loaded onto a TEM specimen holder (PicoFemto) integrated with mobile electrical biasing probe. During the transferring of the holder into the TEM chamber, the lithium metal was intentionally exposed to air (less than 10 s) to form a thin passivation layer of LiO_xN_y on the surface that acted as solid-state electrolyte to allow transport of lithium ions.[15] The images of the LiO_xN_y and low mag images for the raw material and the electrode are shown in Figure S9. No voltage is applied during the first lithium intercalation process (Figure 2) and +1 V voltage is applied during the lithium extraction process (Figure 3).

Data Acquisition and Analysis. The atomic scale STEM images and EDX mapping were acquired at an aberration-corrected FEI (Titan Cubed Themis G2) equipped with an X-FEG gun and a Bruker Super-X EDX detector, operated at 300 kV with the beam current 50 pA, convergence semiangle 21.5 mrad, and collection semiangle snap 80−379 mrad. The quantitative map (Qmap) was conducted to obtain the atomic percentage of V and Se. In situ HRTEM and SAED patterns were carried out at Tecnai F20 at 200 kV. Figures 2 and 3 were acquired by an Oneview IS (Gatan) camera. Figure 4 (ED) were recorded by a Gatan CCD. The atomistic models were generated by Crystalmaker software. The plots were created by Origin 8.5. The FFT patterns and inverse FFT were calculated by DigitalMicrograph (Gatan) software. The simulation of ED was carried by commercial software SingleCrystal 2.3.3 for Windows 8.1 system.

■ ASSOCIATED CONTENT

Supporting Information

The Supporting Information is available free of charge on the ACS Publications website at DOI: 10.1021/acs.nanolett.8b03154.

Figures S1−S9 and Table S1 (PDF)

■ AUTHOR INFORMATION

Corresponding Author

*E-mail: p-gao@pku.edu.cn.

ORCID

Peng Gao: 0000-0003-0860-5525

Notes

The authors declare no competing financial interest.

■ ACKNOWLEDGMENTS

R.W.S. and S.L.C. contributed equally to this work. The work was supported by the National Key R&D Program of China (Grants 2016YFA0300804 and 2016YFA0300903); the National Natural Science Foundation of China (Grants 51502007, 51672007), National Equipment Program of China (ZDYZ2015-1), and China Postdoctoral Science Foundation Funded Project (2017M610010). We gratefully acknowledge Gatan for providing their Oneview IS (Gatan, Inc.) camera as well as the technique help. P.G. also thanks the support from the National Program for Thousand Young Talents of China and "2011 Program" Peking-Tsinghua-IOP Collaborative Innovation Center of Quantum Matter. The authors acknowledge Electron Microscopy Laboratory in Peking University for the use of Cs corrected electron microscope.

■ REFERENCES

(1) Acerce, M.; Voiry, D.; Chhowalla, M. *Nat. Nanotechnol.* **2015**, *10* (4), 313−318.

(2) Radisavljevic, B.; Radenovic, A.; Brivio, J.; Giacometti, V.; Kis, A. *Nat. Nanotechnol.* **2011**, *6* (3), 147.

(3) Wu, S.; Buckley, S.; Schaibley, J. R.; Feng, L.; Yan, J.; Mandrus, D. G.; Hatami, F.; Yao, W.; Vučković, J.; Majumdar, A.; et al. *Nature* **2015**, *520* (7545), 69−72.

(4) Wu, J.; Schmidt, H.; Amara, K. K.; Xu, X.; Eda, G.; Özyilmaz, B. *Nano Lett.* **2014**, *14* (5), 2730.

(5) Wang, H.; Lu, Z.; Kong, D.; Sun, J.; Hymel, T. M.; Cui, Y. *ACS Nano* **2014**, *8* (5), 4940−4947.

(6) Wang, Q. H.; Kalantarzadeh, K.; Kis, A.; Coleman, J. N.; Strano, M. S. *Nat. Nanotechnol.* **2012**, *7* (11), 699−712.

(7) Chhowalla, M. *Chem. Soc. Rev.* **2015**, *44* (9), 272−2712.

(8) Cheng, Y.; Nie, A.; Zhang, Q.; Gan, L. Y.; Shahbazian-Yassar, R.; Schwingenschlogl, U. *ACS Nano* **2014**, *8* (11), 11447.

(9) Wang, C.; He, Q.; Halim, U.; Liu, Y.; Zhu, E.; Lin, Z.; Xiao, H.; Duan, X.; Feng, Z.; Cheng, R.; Weiss, N. O.; Ye, G.; Huang, Y.; Wu, H.; Cheng, H.; Shakir, I.; Liao, L.; Chen, X.; Goddard, W. A., III; Huang, Y.; Duan, X. *Nature* **2018**, *555* (7695), 231−236.

(10) Wang, X.; Shen, X.; Wang, Z.; Yu, R.; Chen, L. *ACS Nano* **2014**, *8* (11), 11394.

(11) Wang, H.; Yuan, H.; Sae Hong, S.; Li, Y.; Cui, Y. *Chem. Soc. Rev.* **2015**, *44* (9), 2664−2680.

(12) Gao, P.; Wang, L.; Zhang, Y. Y.; Huang, Y.; Liu, K. *ACS Nano* **2015**, *9* (11), 11296−301.

(13) Gao, P.; Zhang, Y. Y.; Wang, L.; Chen, S.; Huang, Y.; Ma, X.; Liu, K.; Yu, D. *Nano Energy* **2017**, *32*, 302−309.

(14) Gao, P.; Wang, L.; Zhang, Y. Y.; Huang, Y.; Liao, L.; Sutter, P.; Liu, K.; Yu, D.; Wang, E. G. *Nano Lett.* **2016**, *16* (9), 5582−5588.

(15) Chen, S.; Wang, L.; Shao, R.; Zou, J.; Cai, R.; Lin, J.; Zhu, C.; Zhang, J.; Xu, F.; Cao, J.; Feng, J.; Qi, J.; Gao, P. *Nano Energy* **2018**, *48*, 560−568.

(16) Xiong, F.; Wang, H.; Liu, X.; Sun, J.; Brongersma, M.; Pop, E.; Cui, Y. *Nano Lett.* **2015**, *15* (10), 6777.

(17) Whittingham, M. S. *Mater. Res. Bull.* **1978**, *13* (9), 959−965.

(18) Bao, W.; Wan, J.; Han, X.; Cai, X.; Zhu, H.; Kim, D.; Ma, D.; Xu, Y.; Munday, J. N.; Drew, H. D.; et al. *Nat. Commun.* **2014**, *5* (1), 4224.

(19) Wan, J.; Bao, W.; Liu, Y.; Dai, J.; Shen, F.; Zhou, L.; Cai, X.; Urban, D.; Li, Y.; Jungjohann, K. *Adv. Energy Mater.* **2015**, *5* (5), 1401742.

(20) Yao, J.; Koski, K. J.; Luo, W.; Cha, J. J.; Hu, L.; Kong, D.; Narasimhan, V. K.; Huo, K.; Cui, Y.; et al. *Nat. Commun.* **2014**, *5*, 5670.

(21) Kappera, R.; Voiry, D.; Yalcin, S. E.; Branch, B.; Gupta, G.; Mohite, A. D.; Chhowalla, M. *Nat. Mater.* **2014**, *13* (12), 1128.

(22) Lu, N.; Zhang, P.; Zhang, Q.; Qiao, R.; He, Q.; Li, H.; Wang, Y.; Guo, J.; Zhang, D.; Duan, Z.; et al. *Nature* **2017**, *546* (7656), 124.

DOI: 10.1021/acs.nanolett.8b03154
Nano Lett. 2018, 18, 6094−6099

(23) Wang, Y.; Xiao, J.; Zhu, H.; Li, Y.; Alsaid, Y.; Fong, K. Y.; Zhou, Y.; Wang, S.; Shi, W.; Wang, Y.; et al. *Nature* **2017**, *550* (7677), 487.
(24) Yu, Y.; Yang, F.; Lu, X. F.; Yan, Y. J.; Cho, Y.; Ma, L.; Niu, X.; Kim, S.; Son, Y.; Feng, D.; et al. *Nat. Nanotechnol.* **2015**, *10* (3), 270.
(25) Pettenkofer, C.; Jaegermann, W. *Phys. Rev. B: Condens. Matter Mater. Phys.* **1994**, *50* (12), 8816.
(26) Rossnagel, K. *New J. Phys.* **2010**, *12* (12), 125018.
(27) Ang, R.; Tanaka, Y.; Ieki, E.; Nakayama, K.; Sato, T.; Li, L. J.; Lu, W. J.; Sun, Y. P.; Takahashi, T. *Phys. Rev. Lett.* **2012**, *109* (17), 176403.
(28) Ye, J. T.; Zhang, Y. J.; Akashi, R.; Bahramy, M. S.; Arita, R.; Iwasa, Y. *Science* **2012**, *338* (6111), 1193−1196.
(29) Lu, J. M.; Zheliuk, O.; Leermakers, I.; Yuan, N. F.; Zeitler, U.; Law, K. T.; Ye, J. T. *Science* **2015**, *350* (6266), 1353−1357.
(30) Podzorov, V.; Gershenson, M. E.; Kloc, C.; Zeis, R.; Bucher, E. *Appl. Phys. Lett.* **2004**, *84* (17), 3301−3303.
(31) Zhang, Y.; Ye, J.; Matsuhashi, Y.; Iwasa, Y. *Nano Lett.* **2012**, *12* (3), 1136−1140.
(32) Yuan, H.; Bahramy, M. S.; Morimoto, K.; Wu, S.; Nomura, K.; Yang, B. J.; Shimotani, H.; Suzuki, R.; Toh, M.; Kloc, C.; et al. *Nat. Phys.* **2013**, *9* (9), 563−569.
(33) Zhang, Y. J.; Oka, T.; Suzuki, R.; Ye, J. T.; Iwasa, Y. *Science* **2014**, *344* (6185), 725.
(34) Wang, C.; Xu, W.; Liu, J.; Zhang, J.; Saraf, L. V.; Arey, B. W.; Choi, D.; Yang, Z.; Xiao, J.; Thevuthasan, S.; et al. *Nano Lett.* **2011**, *11* (5), 1874−1880.
(35) Liu, X. H.; Wang, J. W.; Huang, S.; Fan, F.; Huang, X.; Liu, Y.; Krylyuk, S.; Yoo, J.; Dayeh, S. A.; Davydov, A. V.; et al. *Nat. Nanotechnol.* **2012**, *7* (11), 749−756.
(36) Zhu, Y.; Wang, J. W.; Liu, Y.; Liu, X.; Kushima, A.; Liu, Y.; Xu, Y.; Mao, S. X.; Li, J.; Wang, C.; et al. *Adv. Mater.* **2013**, *25* (38), 5461−5466.
(37) Huang, J. Y.; Zhong, L.; Wang, C. M.; Sullivan, J. P.; Xu, W.; Zhang, L. Q.; Mao, S. X.; Hudak, N. S.; Liu, X. H.; Subramanian, A.; et al. *Science* **2010**, *330* (6010), 1515−1520.
(38) Silbernagel, B. G.; Thompson, A. H.; Gamble, F. R. *AIP Conference Proceedings. AIP* **1975**, *24* (1), 380−381.
(39) Lewis, L. H.; Goodenough, J. B. *J. Solid State Chem.* **1995**, *114* (2), 342−345.
(40) Schneemeyer, L. F.; Stacy, A.; Sienko, M. *Inorg. Chem.* **1980**, *19* (9), 2659−2662.
(41) He, S.; Lin, H.; Qin, L.; Mao, Z.; He, H.; Li, Y.; Li, Q. *J. Mater. Chem. A* **2017**, *5* (5), 2163−2171.
(42) Falmbigl, M.; Putzky, D.; Ditto, J.; Johnson, D. C. *J. Solid State Chem.* **2015**, *231*, 101−107.
(43) Spiecker, E.; Schmid, A. K.; Minor, A. M.; Dahmen, U.; Hollensteiner, S.; Jäger, W.; et al. *Phys. Rev. Lett.* **2006**, *96* (8), 086401.
(44) Bayard, M.; Sienko, M. J. *J. Solid State Chem.* **1976**, *19* (4), 325−329.
(45) Wiegers, G. A. *J. Phys. C: Solid State Phys.* **1981**, *14* (29), 4225.
(46) Fang, C. M.; Van Bruggen, C. F.; De Groot, R. A.; Wiegers, G. A.; Haas, C.; et al. *J. Phys.: Condens. Matter* **1997**, *9* (46), 10173.
(47) Poddar, P.; Rastogi, A. K. *J. Phys.: Cond. Matter* **2002**, *14* (10), 2677.
(48) Fujimori, A.; Saeki, M.; Nozaki, H. *Phys. Rev. B: Condens. Matter Mater. Phys.* **1991**, *44* (1), 163.
(49) Knecht, M.; Ebert, H.; et al. *J. Phys.: Condens. Matter* **1998**, *10* (42), 9455.
(50) Chen, X.; Wang, X.; Wang, Z.; Yu, W.; Qian, Y. *Mater. Chem. Phys.* **2004**, *87* (2−3), 327−331.
(51) Li, F.; Tu, K.; Chen, Z. *J. Phys. Chem. C* **2014**, *118* (36), 21264−21274.
(52) Wang, Y.; Sofer, Z.; Luxa, J.; Pumera, M. *Adv. Mater. Interfaces* **2016**, *3* (23), 1600433.
(53) Bayard, M.; Sienko, M. J. *J. Solid State Chem.* **1976**, *19* (4), 325−329.
(54) Thompson, A. H.; Silbernagel, B. G. *Phys. Rev. B: Condens. Matter Mater. Phys.* **1979**, *19* (7), 3420−3426.
(55) van Bruggen, C. F.; Haas, C. *Solid State Commun.* **1976**, *20* (3), 251−254.
(56) DiSalvo, F. J.; Waszczak, J. V. *Phys. Rev. B: Condens. Matter Mater. Phys.* **1981**, *23* (2), 457−461.
(57) Oka, Y.; Kosuge, K.; Kachi, S. *J. Solid State Chem.* **1978**, *23* (1), 11−18.
(58) Ohtani, T.; Fujimoto, R.; Yoshinaga, H.; Nakahira, M.; Ueda, Y. *J. Solid State Chem.* **1983**, *48* (2), 161−167.
(59) Poddar, P.; Rastogi, A. K. *J. Phys.: Cond. Matter* **2002**, *14* (10), 2677.
(60) Popma, T.; Van Bruggen, C. F. *J. Inorg. Nucl. Chem.* **1969**, *31* (1), 73−80.
(61) Plovnick, R. H.; Perloff, D. S.; Vlasse, M.; Wold, A. *J. Phys. Chem. Solids* **1968**, *29* (11), 1935−1940.
(62) Katsuta, H.; McLellan, R. B.; Suzuki, K. *J. Phys. Chem. Solids* **1979**, *40* (12), 1089−1091.
(63) Yokoyama, M.; Yoshimura, M.; Wakihara, M.; Somiya, S.; Taniguchi, M. *J. Solid State Chem.* **1985**, *60* (2), 182−187.
(64) Moutaabbid, H.; Le Godec, Y.; Taverna, D.; Baptiste, B.; Klein, Y.; Loupias, G.; Gauzzi, A. *Inorg. Chem.* **2016**, *55* (13), 6481−6486.
(65) Fang, C. M.; Van Bruggen, C. F.; De Groot, R. A.; Wiegers, G. A.; Haas, C. *J. Phys.: Condens. Matter* **1997**, *9* (46), 10173.
(66) Miyauchi, K.; Hayashi, K.; Nakahira, M. *Mater. Res. Bull.* **1983**, *18* (6), 757−764.
(67) Moutaabbid, H.; Le Godec, Y.; Taverna, D.; Baptiste, B.; Klein, Y.; Loupias, G.; Gauzzi, A. *Inorg. Chem.* **2016**, *55* (13), 6481−6486.
(68) Yokoyama, M.; Yoshimura, M.; Wakihara, M.; Somiya, S.; Taniguchi, M. *J. Solid State Chem.* **1985**, *60* (2), 182−187.
(69) Nakazawa, H.; Saeki, M.; Nakahira, M. J. *J. Less-Common Met.* **1975**, *40* (1), 57−63.
(70) Thompson, A. H. *Phys. Rev. Lett.* **1978**, *40* (23), 1511.
(71) McKinnon, W. R.; Dahn, J. R. *Solid State Commun.* **1983**, *48* (1), 43−45.
(72) Peres, J. P.; Weill, F.; Delmas, C. *Solid State Ionics* **1999**, *116* (1−2), 19−27.
(73) Shao-Horn, Y.; Weill, F.; Croguennec, L.; Carlier, D.; Ménétrier, M.; Delmas, C. *Chem. Mater.* **2003**, *15* (15), 2977−2983.

DOI: 10.1021/acs.nanolett.8b03154
Nano Lett. 2018, 18, 6094−6099